



Published in final edited form as:

Neuroimage. 2015 January 1; 0: 89–99. doi:10.1016/j.neuroimage.2014.10.013.

Dynamic Resting State Functional Connectivity in Awake and Anesthetized Rodents

Zhifeng Liang¹, Xiao Liu², and Nanyin Zhang^{1,*}

¹Department of Biomedical Engineering, The Huck Institutes of Life Sciences, The Pennsylvania State University, University Park, PA 16802

²Advanced MRI Section, Laboratory of Functional and Molecular Imaging, NINDS, National Institutes of Health, Bethesda, MD 20892

Abstract

Since its introduction, resting-state functional magnetic resonance imaging (rsfMRI) has been a powerful tool for investigating functional neural networks in both normal and pathological conditions. When measuring resting-state functional connectivity (RSFC), most rsfMRI approaches do not consider its temporal variations and thus only provide the averaged RSFC over the scan time. Recently, there has been a surge of interest to investigate the dynamic characteristics of RSFC in humans, and promising results have been yielded. However, our knowledge regarding the dynamic RSFC in animals remains sparse. In the present study we utilized the single-volume coactivation method to systematically study the dynamic properties of RSFC within the networks of infralimbic cortex (IL) and primary somatosensory cortex (S1) in both awake and anesthetized rats. Our data showed that both IL and S1 networks could be decomposed into several spatially reproducible but temporally changing co-activation patterns (CAPs), suggesting that dynamic RSFC was indeed a characteristic feature in rodents. In addition, we demonstrated that anesthesia profoundly impacted the dynamic RSFC of neural circuits subserving cognitive and emotional functions but had less effects on sensorimotor systems. Finally, we examined the temporal characteristics of each CAP, and found that individual CAPs exhibited consistent temporal evolution patterns. Together, these results suggest that dynamic RSFC might be a general phenomenon in vertebrate animals. In addition, this study has paved the way for further understanding the alterations of dynamic RSFC in animal models of brain disorders.

© 2014 Elsevier Inc. All rights reserved.

*Correspondence Author: Nanyin Zhang, Ph.D, Associate Professor, Department of Biomedical Engineering, The Huck Institutes of the Life Sciences, The Pennsylvania State University, W341 Millennium Science Complex, University Park, PA 16802, Tel: 814-8674791, nuz2@psu.edu.

Financial Disclosures: Authors have no financial conflicts of interest.

Publisher's Disclaimer: This is a PDF file of an unedited manuscript that has been accepted for publication. As a service to our customers we are providing this early version of the manuscript. The manuscript will undergo copyediting, typesetting, and review of the resulting proof before it is published in its final citable form. Please note that during the production process errors may be discovered which could affect the content, and all legal disclaimers that apply to the journal pertain.

Keywords

resting-state functional connectivity; dynamic; rat; medial prefrontal cortex; somatosensory cortex

Introduction

Resting-state functional magnetic resonance imaging (rsfMRI) has revolutionized our understanding of many aspects of human brain networks including their intrinsic functional organizations (Fox et al., 2005; Greicius et al., 2003; Raichle and Snyder, 2007; Wang et al., 2010), developmental and aging profiles (Dosenbach et al., 2010; Pizoli et al., 2011; Smyser et al., 2011; Stevens et al., 2008), and even their genetic basis (Fornito et al., 2011; Hahn et al., 2012; Wiggins et al., 2012). In addition, the plasticity of specific neural circuitries induced by neurobiological behaviors such as learning and memory has been repeatedly revealed by rsfMRI (Albert et al., 2009; Foster and Wilson, 2006; Horowitz et al., 2009). Importantly, alterations in resting-state functional connectivity (RSFC) measured by rsfMRI are tightly linked to numerous neurological, psychiatric and neurodegenerative disorders (Anand et al., 2005; Carter et al., 2012; Greicius et al., 2007; Greicius et al., 2004; Hunter et al., 2012; Kennedy et al., 2006; Lowe et al., 2002; Lustig et al., 2003; Mayer et al., 2011; Tian et al., 2006; van Meer et al., 2012; Whitfield-Gabrieli et al., 2009), suggesting that RSFC can potentially serve as a biomarker for aiding diagnosis and evaluating treatment options for brain diseases (Hong et al., 2009).

Until recently, most rsfMRI approaches measure RSFC by detecting the temporal correlations of spontaneously fluctuating rsfMRI signals (Biswal et al., 1995; Calhoun et al., 2001). These approaches implicitly assume that RSFC was stationary during data acquisitions. Since they do not consider temporal variations of RSFC, in essence they only provide an average of functional connectivity over the recording period. Consequently, important dynamic information may be overlooked with the use of such approaches. Indeed, it has been increasingly recognized that RSFC is dynamic in nature (Allen et al., 2014; Chang and Glover, 2010; Grigg and Grady, 2010; Hutchison et al., 2013b; Keilholz et al., 2013; Magri et al., 2012; Pan et al., 2013; Petridou et al., 2013; Thompson et al., 2013; Thompson et al., 2014). For instance, Chang and Glover elegantly showed that the coherence and phase of functional connectivity between posterior cingulate cortex and the rest of the default mode network varied over time, clearly demonstrating the non-stationary feature of RSFC (Chang and Glover, 2010). In addition, with clustering analysis human brain networks displayed dynamic but quasistable connectivity patterns that diverged substantially from the averaged connectivity pattern (Allen et al., 2014). Importantly, simultaneous electrophysiological and fMRI recordings indicated that time-varying RSFC has neurophysiological origin (Chang et al., 2013; Keilholz, 2014; Magri et al., 2012; Pan et al., 2013; Tagliazucchi et al., 2012b; Thompson et al., 2013; Thompson et al., 2014).

In parallel with promising results of dynamic RSFC yielded in humans, important findings have also been generated in animals. Using a sliding window approach, Hutchison and colleagues observed that RSFC could vary from strongly positive to strongly negative in anesthetized non-human primates, suggesting that dynamic functional connectivity is a

fundamental property in the mammalian brain and cannot be solely attributed to conscious brain processes (Hutchison et al., 2013b). Majeed et. al. also observed spatiotemporal dynamic patterns in the rsfMRI data of anesthetized rats (Majeed et al., 2011; Majeed et al., 2009). Furthermore, recent work by two different groups (Magri et al., 2012; Thompson et al., 2014) demonstrated a relationship between neural activity and spontaneous fluctuations of BOLD signals similar to the one observed in humans (Chang et al., 2013; Tagliazucchi et al., 2012b). Nevertheless, since all these studies were conducted in anesthetized animals, it is difficult to determine the effects of anesthesia on the dynamic RSFC observed. Therefore, in order to bridge the gap between studies in anesthetized animals and awake humans, it is important to study dynamic RSFC in awake animals.

In the present study we employed the single volume co-activation method (Liu and Duyn, 2013) to systematically study the dynamic features of RSFC in awake and anesthetized rodents. This method, based on the notion that spontaneous fluctuations of BOLD signals might be driven by discrete neural events (Petridou et al., 2013; Tagliazucchi et al., 2012a), selects individual rsfMRI frames with the highest seed signal intensity and decomposes these frames into spatially repeatable co-activation patterns (CAPs). With this method we examined the dynamic RSFC in two neural networks—the somatosensory cortex network which is related to the sensorimotor function, and the medial prefrontal cortex network which is involved in cognitive and emotional functions—in both awake and anesthetized rats. In addition, we extended the single volume co-activation method to investigate the temporal characteristics of dynamic RSFC in rodents.

Materials and Methods

Whole brain-coverage rsfMRI data from 42 male Long Evan (LE) rats were acquired in previous studies (Liang et al., 2011, 2012b), and re-analyzed for the purpose of this study. Detailed description of experimental procedures can be found in aforementioned studies. Briefly, all rats were acclimated to the MRI environment and imaging acoustic noise for 7 days as previously described (Liang et al., 2011, 2012a, b; Liang et al., 2013; Zhang et al., 2010) to minimize imaging-related motion and stress. For the imaging setup, rats were briefly anesthetized (2% isoflurane) and secured into a head restrainer with a built-in coil and a body tube. Isoflurane was then discontinued and the whole system was placed into the magnet. Rats were fully awake during imaging sessions. 16 out of 42 rats were also scanned under the anesthetized condition (1.5% isoflurane delivered through a nose cone), which were conducted at least 7 days apart from awake imaging sessions. During anesthetized sessions, the body temperature of the animal was monitored and maintained at $37^{\circ}\text{C} \pm 0.5^{\circ}\text{C}$.

All MRI experiments were conducted on a Bruker 4.7 T magnet with a dual ^1H radiofrequency coil configuration (Insight NeuroImaging Systems, Worcester, MA) consisting of a volume coil for excitation and a surface coil for receiving MRI signals. For each MRI session, RARE sequence was used to acquire anatomical images with the following parameters: TR = 2125ms, TE = 50ms, matrix size = 256×256 , FOV = $3.2\text{cm} \times 3.2\text{cm}$, slice number = 18, slice thickness = 1mm, and RARE factor = 8. Gradient-echo images were then acquired using the echo-planar imaging (EPI) sequence with the

following parameters: TR = 1s, TE = 30ms, flip angle = 60°, matrix size = 64×64, FOV = 3.2cm×3.2cm, slice number=18, and slice thickness = 1mm. 200 volumes were acquired for each rsfMRI run, and six to nine runs were obtained for each session.

The first 10 volumes of each run were removed to ensure the magnetization to reach steady state. rsfMRI images were preprocessed with conventional procedures: registration to a segmented rat brain atlas with MIVA (<http://ccni.wpi.edu/>), motion correction with SPM8 (Wellcome Department of Cognitive Neurology, London, UK), spatial smoothing (FWHM=1mm), regressions of motion parameters and white matter/ventricle signals, band-pass filtering (0.002-0.1 Hz). rsfMRI runs with excessive motion (maximum within-scan displacement >0.5mm) were discarded. For each run, the blood-oxygenation-level dependent (BOLD) signal was mean-removed and normalized by its standard deviation for each voxel. The seed of bilateral infralimbic cortex (IL) was anatomically defined (17 voxels) based on the segmented rat brain atlas in MIVA, and the seed of unilateral primary somatosensory cortex barrel field (S1BF) was manually drawn (12 voxels) based on the Swanson rat atlas (Swanson, 2004). For each seed, the regionally averaged time series was extracted as the reference time course, and rsfMRI frames with the highest 15% BOLD signal intensity in the reference time course were selected. These steps were carried out in individual runs. Selected frames were concatenated, and then averaged to generate the grand-mean CAP for the seed. Subsequently, concatenated frames were clustered into individual CAPs using k-means clustering. To improve the signal-to-noise ratio, we adopted the thresholding method described in Liu et al. prior to the clustering procedure (Liu and Duyn, 2013). Only the top 15% most activated voxels and the bottom 5% most deactivated voxels with a cluster size of minimal 8 voxels were retained for each frame before entering k-means clustering. The k-means clustering was performed using spatial correlation as the distance measure with 100 replications. We evaluated the quality of clustering using the averaged silhouette values. The result showed the choice of 3 clusters had the second highest averaged silhouette value, just slightly lower than the choice of 2 clusters (0.0152 for 2 clusters, 0.0129 for 3 clusters, 0.0115 for 6 clusters and 0.0097 for 10 clusters). In light of the study by Liu et al (Liu et al., 2014), the numbers of clusters were set at 3 (please also see more discussion on this issue in Discussion). Frames within each cluster were averaged to obtain the mean CAP for the cluster. The emergence rate of each CAP was calculated as the ratio between the number of frames in the cluster and the total number of selected frames (15% of all frames) for each seed. To evaluate the homogeneity of each cluster, the index of within-cluster similarity was calculated as the averaged spatial correlation coefficient between the cluster-wise mean CAP and individual frames within the cluster.

To further explore the temporal properties of individual CAPs, each cluster-mean CAP map was used as a spatial template, and the spatial correlation coefficients (SCCs) between each individual rsfMRI frame and the template was calculated using Pearson correlation, resulting in a time series of SCC (i.e. r values) for the CAP. Before calculating the spatial correlation, rsfMRI frames were thresholded using the same method mentioned above (Liu and Duyn, 2013). Subsequently, local SCC peaks were identified by the following steps: 1) the total number of selected peak frames (N_{total}) was set at 2% of all frames, 2) the number of selected peak frames for each cluster (N_{cluster}) was set at $N_{\text{total}} \times$ emergence rate of the cluster, 3) N_{cluster} frames with the highest SCC in each cluster were selected as peak frames

for the cluster, and 4) if one frame was selected as a peak in multiple clusters, it was assigned to the cluster with the highest SCC. Each local peak frame was defined as Time 0 ($t=0$) for an epoch, which also included 5 frames before and 10 frames after $t=0$. All epochs of the same CAP were time-lock averaged to reveal the temporal evolution pattern of the CAP. To assess the relative temporal consistency among these epochs, the variance (S.E.M.) at each time point of synchronized epochs for the same CAP was calculated.

To evaluate the effects of motion on dynamic RSFC, a correlation analysis was performed between the volume-to-volume displacement and the BOLD time series of individual voxels across all runs and animals. The correlation coefficient maps were then averaged across all runs and animals to generate the mean correlation map. Also similar to the concept of generating individual CAPs, 15% rsfMRI frames with the largest motion (i.e. volume-to-volume displacement) were selected and then averaged. In addition, to evaluate the impact of different motion levels on dynamic RSFC between awake and anesthetized rats, a subset of awake animal rsfMRI data was selected by setting an extremely high threshold of motion level (maximum within-scan displacement $<0.2\text{mm}$). In this subset of data (41 scans, approximately 11% of the entire awake animal dataset), the animals' motion level was similar to that in the anesthetized rat (mean maximum within-scan displacement: 0.170mm in awake vs 0.171mm in anesthetized states, $p = 0.88$, two-sample t-test). The same analysis was conducted on this subset of data. To evaluate the impact of physiological noise (e.g. cardiac and respiratory fluctuations), we also examined the spatial pattern of the correlation between the signal averaged from white matter and ventricles and all voxel time series.

Results

Averages of selected rsfMRI frames replicate the RSFC patterns obtained by correlation analysis

The human study employing the single-volume co-activation method indicated that RSFC patterns can be robustly replicated by averaging a portion of rsfMRI time frames (Liu and Duyn, 2013). To confirm this notion in animals, anatomically defined regions of interest (ROIs) including bilateral IL and unilateral S1BF were used as seeds. Our data clearly demonstrated that RSFC patterns obtained from correlational analysis closely resembled the averages of 15% rsfMRI frames (9996 frames for the awake state and 2632 frames for the anesthetized state) with the highest BOLD signal intensity at seed regions (Figures 1 and 2), regardless of the seed location (S1BF or IL) or the brain state (awake or anesthetized). Specifically, in IL maps both methods produced virtually identical co-activation (Fig. 1a) or correlation (Fig. 1b) patterns in widespread regions, including cortical areas like anterior cingulate cortex (ACC), retrosplenium (RSP), subiculum (SUB), somatosensory (SS), motor (MO), prelimbic (PL) and orbital cortices (OC), caudate-putamen (CPu), hypothalamus (HT), as well as limbic structures like amygdala (AMYG), medial dorsal thalamus (MED), nucleus accumbens (NAcc) and septum in awake rats. In the anesthetized state, both the co-activation (Fig. 1c) and correlation (Fig. 1d) were consistently weaker with constricted spatial extent, compared with the awake state (Figure 1c and d). The spatial correlation coefficients between the grand-mean CAPs and correlation maps were 0.997 ($p < 10^{-10}$, uncorrected) and 0.96 ($p < 10^{-10}$, uncorrected) in the awake and anesthetized states,

respectively, again confirming that almost identical RSFC patterns can be revealed by the two methods. For the unilateral S1BF seed, both methods revealed robust co-activation (Fig. 2a) or correlation between left and right S1 in the awake state (Fig. 2b). Similar patterns were also identified in the anesthetized state using both methods (Fig. 2c and d). The spatial correlation coefficients between the S1BF grand-mean CAPs and correlation maps were 0.99 ($p < 10^{-10}$, uncorrected) and 0.98 ($p < 10^{-10}$, uncorrected) in awake and anesthetized rats, respectively. Taken together, these results validated the notion that stationary connectivity patterns (i.e. correlation maps) can be readily revealed by averaging a portion of rsfMRI frames (i.e. grand-mean CAPs). This conclusion can be extended from humans (Liu and Duyn, 2013) to animals in drastically different physiological states.

Dynamic co-activation patterns revealed by temporal clustering of selected rsfMRI frames

Subsequently, we examined the dynamic characteristics of IL and S1BF coactivation patterns. The 15% rsfMRI frames selected for each seed were clustered into multiple CAPs by using the *k*-means clustering approach. Strikingly, for both seeds distinct but repeatable CAPs were observed with strong departures from the grand-mean co-activation or correlation patterns (Figures 3 and 4). Specifically, three spatially reproducible CAPs were identified for IL (Fig. 3a) in the awake state. In CAP1, the strongest co-activation was observed mainly in limbic regions including AMYG, MED, NAcc and septum, as well as the prefrontal regions including ACC, PL and OC, implying this CAP may primarily subservise the function of emotional regulation. 52.8% of total selected frames exhibited this co-activation pattern. In CAP2, the strongest co-activation was observed in the cortical ribbon including motor and somatosensory cortices, as well as CPu. This CAP occurred in 29% of total selected frames. CAP3 showed strong coactivation in hippocampus (HP) with the emergence rate of 18.2%. For the anesthetized state, individual CAPs showed significant changes relative to the awake state (Fig. 3b). In CAP1, the co-activation between IL and limbic regions including AMYG, NAcc, MED and septum observed in the awake state diminished in the anesthetized state. In CAP2, the connectivity between IL and wide spread cortical regions persisted but appeared weaker in the anesthetized state. In CAP3, the co-activation between IL and HP virtually disappeared in anesthetized rats. In addition, the within-cluster similarity was lower for all three CAPs in anesthetized rats (Figure 3), further indicating that anesthesia decreased the synchronization of neural activities within each CAP. Further, anesthesia also impacted the temporal dynamics of individual CAPs in the IL network. The emergence rates substantially decreased for CAP1 (52.8% vs 30.5%) and increased for CAP3 (18.2% vs 37.7%) in anesthetized rats. Notably, the anesthesia-induced difference in the co-activation strength was more pronounced in individual CAPs than the grand-mean CAP. For instance, CAP3 displayed significantly reduced IL-HP coactivation in the anesthetized state than the awake state, whereas the grand-mean CAP did not show any appreciable changes (Figure 5). This result suggests that dynamic RSFC can reveal more subtle connectivity changes than stationary RSFC.

Similarly, three distinct CAPs were identified for the S1BF network (Figure 4). In the awake state (Fig. 4a), CAP1 displayed co-activation in widespread sensorimotor regions, CPu, as well as the prefrontal regions like medial prefrontal and orbital cortices; CAP2 exhibited co-activation in bilateral primary SS cortex; and CAP3 specifically highlighted the co-

activation in part of HP. Among the 15% rsfMRI frames selected for S1BF, CAP1 and CAP2 had similar emergence rates (36.7% and 35.9%, respectively), and the emergence rate for CAP3 was slightly lower (27.4%). The corresponding CAPs in the anesthetized state (Fig. 4b) were generally consistent with those in the awake state, with the exception of CAP3 losing the hippocampal co-activation. Also interestingly, anesthesia-induced differences in emergence rates and within-cluster similarity for individual CAPs in the S1BF network were not as noticeable as the IL network.

All these results collectively indicate that RSFC networks, identified based on the stationarity assumption, can be decomposed into several quasi-stable sub-networks that dynamically alternate. In addition, our data also suggest anesthesia can selectively affect the dynamic RSFC of different networks, more profoundly impacting the neural circuits subserving cognitive and emotional functions than sensorimotor systems.

Temporal characteristics of individual CAPs

All individual CAPs identified represented distinct spatial patterns of spontaneous neural activities co-activated with seed regions. Since these co-activation patterns were dynamic from frame to frame, it is also appealing to examine their temporal characteristics. For that purpose, all epochs of the same CAP were time-lock averaged. Figure 6 showed the averaged temporal evolutions for all three IL (Fig. 6a) and S1BF (Fig. 6b) CAPs at both awake and anesthetized states. In general, for each epoch the SCC started from almost zero at -5s, rose to the peak at 0s and decreased to zero after +5s, resulting in the epoch duration of approximately 10s. In addition, relatively small variations at individual time points indicate that the temporal evolutions of individual epochs had consistent patterns. Statistically, SCCs of 9 frames reached statistical significance (one sample t test, $p < 0.01$, Bonferroni corrected) for most CAPs in the awake state. Epochs of the anesthetized state generally had lower SCCs and shorter epoch durations (5 frames reached statistical significance for most CAPs). These results collectively demonstrated that all CAPs had consistent temporal patterns.

To further evaluate the spatiotemporal dynamics of individual CAPs, the spatial maps of each time point of averaged epochs were shown in movies (Supplemental Information: Movie 1, Movie 2 and Movie 3 for IL-CAP1, IL-CAP2 and IL-CAP3, respectively, in awake rats and Movie 4, Movie 5 and Movie 6 for S1BF-CAP1, S1BFCAP2 and S1BF-CAP3, respectively, in awake rats). Consistent with the SCC temporal evolution patterns in Fig. 6, these movies clearly showed a general pattern of rising and falling of co-activation in both spatial extent and amplitude. For instance, the IL CAP1 started with weak co-activation in PL and ACC at -5s. This co-activation strengthened and spread to CPU and orbital cortex at -4s. At -3s, AMYG, thalamus and other cortical regions started to display co-activation with IL. The strongest co-activation in all regions occurred at 0s (i.e. peak SCC). After 0s, co-activation started to weaken and gradually disappeared following a reversed time pattern, starting from the disappearance of coactivation at thalamus, AMYG and cortical regions, followed by CPU and OC. ACC and PL remained weakly co-activated until +6s. Similar patterns were seen in IL CAP2 and CAP3.

Influences of motion and physiologic noise on dynamic RSFC

To rule out the possibility that the dynamic RSFC observed in awake rats originated from motion, we further analyzed the temporal relationship between animals' movement and the BOLD time series of individual voxels. Figure 7a shows distinct temporal patterns between seed time courses (blue curve for IL and magenta curve for S1BF) and the volume-to-volume displacement (green curve) from a randomly selected rsfMRI scan. Figure 7b shows the averaged map of the correlation coefficient between the volume-to-volume displacement and the unfiltered BOLD time series of each individual voxel (i.e. with all preprocessing steps except for temporal filtering). Figure 7c shows the histogram of averaged correlation coefficients across all voxels. The data indicate that this correlation was very weak across the whole brain, and no significant spatial patterns were observed. Figure 7d shows the grand-mean CAP from 15% rsfMRI frames with the largest volume-to-volume movement, and again, no obvious motion-related spatial patterns were observed. Taken together, these results unequivocally suggest that motion did not significantly contribute to the dynamic RSFC patterns observed in awake rats.

To further demonstrate that differences in dynamic RSFC between the awake and anesthetized rats were not caused by different motion levels in the two groups, we selected a subset of the awake rat dataset. This subset of data had a similar motion level to that in the anesthetized rat (see **Materials and Methods**). The same analysis was conducted on this subset of data, and the results were very consistent with those obtained from the complete dataset (Supplemental Fig. 1 and 2, including the average of 15% rsfMRI frames as well as individual CAPs for both IL and S1BF seeds). These results indicate that different motion levels did not cause the differences in CAPs between awake and anesthetized states.

To demonstrate that the CAPs obtained were not mainly effects of physiological noise, we calculated the correlation between the BOLD signals from the white matter and ventricles, which were presumably dominated by physiologic noise (Chai et al., 2012; Chang and Glover, 2009), and the BOLD time series of individual voxels (Supplemental Fig 3). The spatial pattern of this correlation departed far away from any CAPs reported in the current study. This result shows that physiological factors did not account for any major effects in the coactivation patterns observed in the present study.

Discussion

In the present study we systematically investigated the spatiotemporal characteristics of dynamic RSFC in awake and anesthetized animals using the single volume co-activation method. Firstly, we examined the spatial patterns of dynamic RSFC for the seed regions of IL and S1BF. Grand-mean CAPs obtained by averaging 15% rsfMRI frames with the highest seed signal intensity closely resembled the RSFC maps generated from conventional seed-based correlational analysis (Liu and Duyn, 2013). The *k*-means clustering approach further revealed distinct CAPs that were not apparent in grand-mean CAPs. Importantly, these temporally changing CAPs were spatially repeatable, suggesting the IL and S1BF RSFC networks can be decomposed into several discrete but recurring subnetworks. Secondly, we studied the specific effects of anesthesia on the dynamic RSFC in both IL and S1BF networks. We found that anesthesia selectively impacted neural circuits subserving

cognitive and emotional functions, albeit exerted less influences on sensorimotor systems. Lastly, we showed that individual CAPs had consistent temporal patterns. Taken together, these results provide direct answers to three critical questions regarding dynamic RSFC in animals. First, is dynamic RSFC a characteristic feature in the animal brain? Second, how does anesthesia affect dynamic RSFC? Third, does dynamic RSFC manifest quasi-stable connectivity (Allen et al., 2014) patterns or varies along a continuous spectrum?

Spatiotemporal patterns of dynamic RSFC in the rat brain

Although dynamic RSFC has been demonstrated in humans (Chang and Glover, 2010; Liu and Duyn, 2013), a critical question to be addressed is whether time-varying RSFC is also a characteristic property of the animal brain. Previous studies have shown dynamic RSFC in anesthetized monkeys (Hutchison et al., 2013b) and rats (Majeed et al., 2011; Majeed et al., 2009; Thompson et al., 2013; Thompson et al., 2014). However, it is unclear to what extent the dynamic RSFC reported was modulated by anesthesia itself, especially considering the fact that anesthesia can profoundly change RSFC (Liang et al., 2012a, b; Liu et al., 2011; Lu et al., 2007). The present study extended the previous work by eliminating the confounding factor of anesthesia and investigating the dynamic properties of RSFC in awake rodents. Our data showed that both IL and S1BF networks clearly displayed spatially reproducible but temporally changing CAPs that diverged substantially from the stationary connectivity patterns (Figs. 3 and 4), suggesting that RSFC was indeed dynamic in the awake rodent brain. Combining with the findings in humans and non-human primates (Allen et al., 2014; Hutchison et al., 2013b; Liu and Duyn, 2013), our results indicate that dynamic RSFC might be a general phenomenon in vertebrate animals.

Another important question regarding the spatiotemporal dynamics of RSFC is to what extent dynamic RSFC can be described as a multistable state space where in discrete CAPs repeatedly occur or whether dynamic RSFC simply varies along a continuous spectrum (Hutchison et al., 2013a). Human studies have begun to identify discrete, reproducible patterns of RSFC, providing some evidence of multistability (Allen et al., 2014). Spatially repeatable CAPs for both IL and S1BF networks in our awake rat data, reflected by high within-cluster similarity for all CAPs, also support this hypothesis (Hutchison et al., 2013a). However, a thorough test of this hypothesis needs to examine the consistency of both spatial and temporal patterns of individual CAPs. Hence, the present study examined the temporal patterns of CAPs by determining the SCC between each individual frame and CAP templates. Our results indicated that an epoch for each CAP lasted approximately 10s and the temporal evolution pattern was consistent within and across CAPs. In addition, this time scale of CAP epochs also agrees with the time period of spatiotemporal dynamic patterns observed in anesthetized rats in a separate study using a different approach (Majeed et al., 2011). Together, these results showed discrete CAPs for IL and S1BF networks that were spatially and temporally repeatable, indicating that RSFC networks in rodents also demonstrated dynamic but quasi-stable subnetworks as shown in human studies (Allen et al., 2014).

Notably, epoch durations of was identified based on the rsfMRI measurement. Considering the temporal smoothing effects of hemodynamic responses, the underlying spontaneous

neural activities might be faster. Indeed, with the voltage-sensitive dye imaging method spontaneous cortical co-activation was reported in the order of hundreds of milliseconds in awake and anesthetized mice (Mohajerani et al., 2013). Similarly, a recent human MEG study suggested shorter durations (100-200ms) for spontaneous brain states (Baker et al., 2014). By taking in account slow hemodynamic responses and the low-pass filtering applied in data preprocessing, the epoch duration identified in the present study (~10s) may suggest that the underlying co-activated spontaneous neural activities might be brief (on the order of a few seconds), compared the common resting-state scan length (on the order of minutes). Indeed, when the same analysis was performed on unfiltered data (i.e. with all preprocessing steps except for temporal filtering), the durations of epochs were decreased to around 4 seconds (Supplemental Figure 4). In addition to the smoothing effect of temporal filtering, this difference may also arise from different noise levels between the filtered and unfiltered data, or the possibility that spontaneous activity in one frequency may drive it in other frequencies (Raichle, 2011).

Impact of anesthesia on dynamic RSFC

Since dynamic RSFC was observed in the awake as well as anesthetized states, it would be appealing to examine how anesthesia impacted dynamic RSFC in animals. In the present study we specifically compared individual CAPs of IL and S1BF networks between anesthetized and awake animals. Consistent with the literature report (Liang et al., 2012a, b; Liu et al., 2011; Lu et al., 2007), the connectivity strength was on average weakened in most CAPs in the anesthetized state. Intriguingly, anesthesia did not uniformly change the connectivity strength across all CAPs. The influences were more pronounced in neural circuits subserving cognitive and emotional functions than those involved in sensorimotor functions. For instance, bilateral somatosensory co-activation was weaker but still appreciable in the anesthetized state (S1BF-CAP2, Fig. 4), and similar patterns were also observed in previous studies on anesthetized rats (Majeed et al., 2011; Majeed et al., 2009; Thompson et al., 2013). By contrast, IL-HP (IL-CAP1, Fig. 3) co-activation virtually vanished in the anesthetized rat. These results support the concept that cognitive and emotional regulations are generally disabled while sensorimotor systems may still be functioning at anesthetized states.

Dynamic RSFC can provide more subtle connectivity information

An important advantage of dynamic RSFC approaches is that they can detect more specific connectivity changes (Sakoglu et al., 2010) than conventional methods based on the stationarity assumption. This notion was clearly validated in the present study. In the IL map generated by the correlational analysis, no appreciable RSFC between IL and HP was observed. However, the functional connectivity between IL and HP in rodents has been well established in the literature (Vertes, 2004). This contradiction can be well reconciled by the dynamic RSFC approach applied here, which indeed identified appreciable functional connectivity between IL and HP (ILCAP3), although this connectivity only occurred in 18.2% of the total acquisition time. As stationary approaches averaged RSFC across the entire acquisition period, this dynamic IL-HP connectivity most likely diminished in stationary RSFC maps. Besides, anesthesia had a significant impact on the dynamic RSFC

between IL and HP, and this change was only detectable using the dynamic RSFC approach (Fig. 5).

In addition to the co-activation strength, other metrics were also useful for revealing RSFC differences in different states. For example, all IL CAPs had lower within-cluster similarity in the anesthetized state compared to the awake state, which was not the case for S1BF CAPs. This observation indicates the quasi-stable states of the IL network were not as robust as the S1BF network in the anesthetized state, again pointing to the notion that anesthesia impacts cognitive and emotional networks more significantly than the sensorimotor networks. Further, emergence rates may also help reveal or interpret RSFC changes in different states. As averaged connectivity maps are essentially weighted combinations of all individual CAPs, differences in emergence rates for individual CAPs can potentially explain the changes in averaged connectivity maps at distinct conditions. Taken together, our results provide evidence suggesting that dynamic RSFC approaches can provide connectivity information from multiple dimensions and contain higher sensitivity to reveal more subtle connectivity changes.

Influences of physiological noise and motion on dynamic RSFC

Estimating the dynamics of RSFC is particularly sensitive to noise. Time varying physiological fluctuations and motion can generate spatially correlated signals and be misinterpreted as 'dynamic RSFC'. However, we believe the contributions of physiologic noise to our results were very minor in the present study. First, a recent publication showed that the relative contributions from cardiac and respiratory noise to the rsfMRI signal were 1% and 5%, respectively, in the rat (Kalthoff et al., 2011). Second, we filtered out high-frequency signals by setting the threshold of the low-pass filter at 0.1 Hz for both awake and anesthetized rats. As a result, the impact of respiratory and cardiac effects on RSFC should be greatly diminished. Also in image preprocessing we regressed out the signals from the white matter and ventricles to further minimize the influences of physiologic noise (Chang and Glover, 2009). Third, we calculated the correlation between the BOLD signals from the white matter and ventricles and the time series of each individual voxels (Supplemental Fig 3). The spatial pattern of this correlation departed far away from any CAP patterns reported in the current study, suggesting minimal influences from physiologic noise on the CAPs. These results collectively suggest that physiological noise did not account for any major effects of dynamic RSFC observed in the present study.

In addition to physiological noise, motion is another important confounding factor that needs to be carefully studied. In the present study, we adopted several preprocessing procedures to control for motion artifacts. First, functional images were realigned with the SPM realignment function. Second, scans with excessive movement (maximum within-scan displacement $>0.5\text{mm}$) were excluded. Third, all six motion parameters were regressed out. With these preprocessing steps, no significant correlation patterns were found between motion parameters and the BOLD signals across the brain (Figure 7). However, even with these widely used criteria, the motion level was still significantly higher in awake rats than anesthetized rats. Therefore, to further evaluate the impact of different motion levels on the differences of dynamic RSFC between awake and anesthetized states, we selected a subset

of the awake animal dataset with similar motion levels to anesthetized rats. Very similar results were observed in this subset of data compared to those obtained from the whole dataset (Supplemental Figure 1 and 2), indicating that the differences in CAPs between awake and anesthetized states cannot be attributed to different motion levels.

Concerns have also been raised that whether dynamic RSFC patterns would result from regional variations of signal to noise ratio (SNR) (Logothetis et al., 2009; Shmuel and Leopold, 2008). In these studies, the spatiotemporal dynamics (e.g. Figure 7 in (Logothetis et al., 2009)) were essentially the correlation between neural signals recorded by electrodes and voxel-wise BOLD time series with different time lags (1-9 s) at a local region (e.g. V1). Thus it is possible that different SNR/CNR due to local vasculatures can cause dynamic patterns observed as regions with high SNR/CNR would show correlation with neural signals first, and regions with low SNR/CNR would show correlation later. However, in the present study all CAP shown were widely distributed across the whole brain with a much larger spatial scale (on the order of cm) than that of the effect from a single vessel (on the order of mm). Therefore, it is unlikely that “regional variations in SNR” were the origin of the observed dynamic patterns.

Potential limitations

One challenge for the k -means clustering analysis is to determine the optimal number of clusters (i.e. the number of CAPs here). In the present study, we evaluated the quality of clustering using the averaged silhouette values. The result showed the choice of 3 clusters had the second highest averaged silhouette value, just slightly lower than the choice of 2 clusters. When 2 clusters were used, the resulting CAPs were very similar to CAPs 1 and 2 reported, but without CAP3 (i.e. the hippocampal CAP). Nevertheless, we believe 3 clusters might still provide a reasonable cluster number, considering the well-defined anatomical location of CAP3 and well-established IL-HP connectivity. In addition, it is possible that the evaluation method based on silhouette values might underestimate the optimal cluster number, as pointed out by Liu et al. (Liu et al., 2014). Considering all these factors, we mainly reported the results based on the cluster number of 3 in the present study. The other limitation of the present study is lack of recordings of cardiac and respiratory rates during rsfMRI scans. At the TR of 1s used in the present study, there were aliasing effects in the rsfMRI signals from physiologic noise. Without the measurement of physiological parameters, it was difficult to determine the exact aliased frequencies of physiological noise. Nevertheless, as discussed above, the influences of physiologic noise on the dynamic RSFC reported in the present study should be very minor.

Summary and Conclusion

In the last two decades, RSFC measured based on the stationarity assumption has been proven useful to understand brain network organization in humans and animals. However, recent research unequivocally suggested that more rich information can be obtained by investigating the dynamic characteristics of RSFC. The present study has provided important insight into understanding the dynamic RSFC in awake and anesthetized rodents. Our data clearly showed that RSFC is intrinsically dynamic in the rat brain. These results are not only useful for understanding neural networks in animals at basal conditions, but also

pave the way for further investigating their dynamic reconfigurations in different animal models of brain disorders (Heffernan et al., 2013; Huang et al., 2011; Liang et al., 2014). Therefore, we might be in a better position to translate findings between animals and humans.

Supplementary Material

Refer to Web version on PubMed Central for supplementary material.

Acknowledgments

We thank Ms. Christina Hamilton for editing the manuscript. The work was also supported by the National Institutes of Health, Grant Numbers R01MH098003 (PI: Nanyin Zhang, PhD) from the National Institute of Mental Health and R01NS085200 (PI: Nanyin Zhang, PhD) from the National Institute of Neurological Disorders and Stroke.

References

- Albert NB, Robertson EM, Miall RC. The resting human brain and motor learning. *Curr Biol*. 2009; 19:1023–1027. [PubMed: 19427210]
- Allen EA, Damaraju E, Plis SM, Erhardt EB, Eichele T, Calhoun VD. Tracking whole-brain connectivity dynamics in the resting state. *Cereb Cortex*. 2014; 24:663–676. [PubMed: 23146964]
- Anand A, Li Y, Wang Y, Wu J, Gao S, Bukhari L, Mathews VP, Kalnin A, Lowe MJ. Activity and connectivity of brain mood regulating circuit in depression: a functional magnetic resonance study. *Biol Psychiatry*. 2005; 57:1079–1088. [PubMed: 15866546]
- Baker AP, Brookes MJ, Rezek IA, Smith SM, Behrens T, Probert Smith PJ, Woolrich M. Fast transient networks in spontaneous human brain activity. *Elife*. 2014; 3:e01867. [PubMed: 24668169]
- Biswal B, Yetkin FZ, Haughton VM, Hyde JS. Functional connectivity in the motor cortex of resting human brain using echo-planar MRI. *Magn Reson Med*. 1995; 34:537–541. [PubMed: 8524021]
- Calhoun VD, Adali T, Pearlson GD, Pekar JJ. A method for making group inferences from functional MRI data using independent component analysis. *Hum Brain Mapp*. 2001; 14:140–151. [PubMed: 11559959]
- Carter AR, Shulman GL, Corbetta M. Why use a connectivity-based approach to study stroke and recovery of function? *Neuroimage*. 2012; 62:2271–2280. [PubMed: 22414990]
- Chai XJ, Castanon AN, Ongur D, Whitfield-Gabrieli S. Anticorrelations in resting state networks without global signal regression. *Neuroimage*. 2012; 59:1420–1428. [PubMed: 21889994]
- Chang C, Glover GH. Effects of model-based physiological noise correction on default mode network anti-correlations and correlations. *Neuroimage*. 2009; 47:1448–1459. [PubMed: 19446646]
- Chang C, Glover GH. Time-frequency dynamics of resting-state brain connectivity measured with fMRI. *Neuroimage*. 2010; 50:81–98. [PubMed: 20006716]
- Chang C, Liu Z, Chen MC, Liu X, Duyn JH. EEG correlates of time-varying BOLD functional connectivity. *Neuroimage*. 2013; 72:227–236. [PubMed: 23376790]
- Dosenbach NU, Nardos B, Cohen AL, Fair DA, Power JD, Church JA, Nelson SM, Wig GS, Vogel AC, Lessov-Schlaggar CN, Barnes KA, Dubis JW, Feczko E, Coalson RS, Pruett JR Jr, Barch DM, Petersen SE, Schlaggar BL. Prediction of individual brain maturity using fMRI. *Science*. 2010; 329:1358–1361. [PubMed: 20829489]
- Fornito A, Zalesky A, Bassett DS, Meunier D, Ellison-Wright I, Yucel M, Wood SJ, Shaw K, O'Connor J, Nertney D, Mowry BJ, Pantelis C, Bullmore ET. Genetic influences on cost-efficient organization of human cortical functional networks. *J Neurosci*. 2011; 31:3261–3270. [PubMed: 21368038]
- Foster DJ, Wilson MA. Reverse replay of behavioural sequences in hippocampal place cells during the awake state. *Nature*. 2006; 440:680–683. [PubMed: 16474382]

- Fox MD, Snyder AZ, Vincent JL, Corbetta M, Van Essen DC, Raichle ME. The human brain is intrinsically organized into dynamic, anticorrelated functional networks. *Proc Natl Acad Sci U S A*. 2005; 102:9673–9678. [PubMed: 15976020]
- Greicius MD, Flores BH, Menon V, Glover GH, Solvason HB, Kenna H, Reiss AL, Schlaggar AF. Resting-state functional connectivity in major depression: abnormally increased contributions from subgenual cingulate cortex and thalamus. *Biol Psychiatry*. 2007; 62:429–437. [PubMed: 17210143]
- Greicius MD, Krasnow B, Reiss AL, Menon V. Functional connectivity in the resting brain: a network analysis of the default mode hypothesis. *Proc Natl Acad Sci U S A*. 2003; 100:253–258. [PubMed: 12506194]
- Greicius MD, Srivastava G, Reiss AL, Menon V. Default-mode network activity distinguishes Alzheimer's disease from healthy aging: evidence from functional MRI. *Proc Natl Acad Sci U S A*. 2004; 101:4637–4642. [PubMed: 15070770]
- Grigg O, Grady CL. Task-related effects on the temporal and spatial dynamics of resting-state functional connectivity in the default network. *PLoS One*. 2010; 5:e13311. [PubMed: 20967203]
- Hahn A, Wadsak W, Windischberger C, Baldinger P, Hoflich AS, Losak J, Nics L, Philippe C, Kranz GS, Kraus C, Mitterhauser M, Karanikas G, Kasper S, Lanzenberger R. Differential modulation of the default mode network via serotonin-1A receptors. *Proc Natl Acad Sci U S A*. 2012; 109:2619–2624. [PubMed: 22308408]
- Heffernan ME, Huang W, Sicard KM, Bratane BT, Sikoglu EM, Zhang N, Fisher M, King JA. Multimodal approach for investigating brain and behavior changes in an animal model of traumatic brain injury. *J Neurotrauma*. 2013; 30:1007–1012. [PubMed: 23294038]
- Hong LE, Gu H, Yang Y, Ross TJ, Salmeron BJ, Buchholz B, Thaker GK, Stein EA. Association of nicotine addiction and nicotine's actions with separate cingulate cortex functional circuits. *Arch Gen Psychiatry*. 2009; 66:431–441. [PubMed: 19349313]
- Horowitz SG, Braun AR, Carr WS, Picchioni D, Balkin TJ, Fukunaga M, Duyn JH. Decoupling of the brain's default mode network during deep sleep. *Proc Natl Acad Sci U S A*. 2009; 106:11376–11381. [PubMed: 19549821]
- Huang W, Heffernan ME, Li Z, Zhang N, Overstreet DH, King JA. Fear induced neuronal alterations in a genetic model of depression: an fMRI study on awake animals. *Neurosci Lett*. 2011; 489:74–78. [PubMed: 21134416]
- Hunter JV, Wilde EA, Tong KA, Holshouser BA. Emerging imaging tools for use with traumatic brain injury research. *J Neurotrauma*. 2012; 29:654–671. [PubMed: 21787167]
- Hutchison RM, Womelsdorf T, Allen EA, Bandettini PA, Calhoun VD, Corbetta M, Della Penna S, Duyn JH, Glover GH, Gonzalez-Castillo J, Handwerker DA, Keilholz S, Kiviniemi V, Leopold DA, de Pasquale F, Sporns O, Walter M, Chang C. Dynamic functional connectivity: promise, issues, and interpretations. *Neuroimage*. 2013a; 80:360–378. [PubMed: 23707587]
- Hutchison RM, Womelsdorf T, Gati JS, Everling S, Menon RS. Restingstate networks show dynamic functional connectivity in awake humans and anesthetized macaques. *Hum Brain Mapp*. 2013b; 34:2154–2177. [PubMed: 22438275]
- Kalthoff D, Seehafer JU, Po C, Wiedermann D, Hoehn M. Functional connectivity in the rat at 11.7T: Impact of physiological noise in resting state fMRI. *Neuroimage*. 2011; 54:2828–2839. [PubMed: 20974263]
- Keilholz SD. The Neural Basis of Time-Varying Resting-State Functional Connectivity. *Brain Connect*. 2014 Epub ahead of print.
- Keilholz SD, Magnuson ME, Pan WJ, Willis M, Thompson GJ. Dynamic properties of functional connectivity in the rodent. *Brain Connect*. 2013; 3:31–40. [PubMed: 23106103]
- Kennedy DP, Redcay E, Courchesne E. Failing to deactivate: resting functional abnormalities in autism. *Proc Natl Acad Sci U S A*. 2006; 103:8275–8280. [PubMed: 16702548]
- Liang Z, King J, Zhang N. Uncovering intrinsic connective architecture of functional networks in awake rat brain. *J Neurosci*. 2011; 31:3776–3783. [PubMed: 21389232]
- Liang Z, King J, Zhang N. Anticorrelated resting-state functional connectivity in awake rat brain. *Neuroimage*. 2012a; 59:1190–1199. [PubMed: 21864689]

- Liang Z, King J, Zhang N. Intrinsic organization of the anesthetized brain. *J Neurosci*. 2012b; 32:10183–10191. [PubMed: 22836253]
- Liang Z, King J, Zhang N. Neuroplasticity to a single-episode traumatic stress revealed by resting-state fMRI in awake rats. *Neuroimage*. 2014 in press.
- Liang Z, Li T, King J, Zhang N. Mapping thalamocortical networks in rat brain using resting-state functional connectivity. *Neuroimage*. 2013; 83:237–244. [PubMed: 2377756]
- Liu X, Duyn JH. Time-varying functional network information extracted from brief instances of spontaneous brain activity. *Proc Natl Acad Sci U S A*. 2013; 110:4392–4397. [PubMed: 23440216]
- Liu X, Yanagawa T, Leopold DA, Fujii N, Duyn JH. Robust Long-Range Coordination of Spontaneous Neural Activity in Waking, Sleep and Anesthesia. *Cereb Cortex*. 2014
- Liu X, Zhu XH, Zhang Y, Chen W. Neural origin of spontaneous hemodynamic fluctuations in rats under burst-suppression anesthesia condition. *Cereb Cortex*. 2011; 21:374–384. [PubMed: 20530220]
- Logothetis NK, Murayama Y, Augath M, Steffen T, Werner J, Oeltermann A. How not to study spontaneous activity. *Neuroimage*. 2009; 45:1080–1089. [PubMed: 19344685]
- Lowe MJ, Phillips MD, Lurito JT, Mattson D, Dzemidzic M, Mathews VP. Multiple sclerosis: low-frequency temporal blood oxygen level-dependent fluctuations indicate reduced functional connectivity initial results. *Radiology*. 2002; 224:184–192. [PubMed: 12091681]
- Lu H, Zuo Y, Gu H, Waltz JA, Zhan W, Scholl CA, Rea W, Yang Y, Stein EA. Synchronized delta oscillations correlate with the resting-state functional MRI signal. *Proc Natl Acad Sci U S A*. 2007; 104:18265–18269. [PubMed: 17991778]
- Lustig C, Snyder AZ, Bhakta M, O'Brien KC, McAvoy M, Raichle ME, Morris JC, Buckner RL. Functional deactivations: change with age and dementia of the Alzheimer type. *Proc Natl Acad Sci U S A*. 2003; 100:14504–14509. [PubMed: 14608034]
- Magri C, Schridde U, Murayama Y, Panzeri S, Logothetis NK. The amplitude and timing of the BOLD signal reflects the relationship between local field potential power at different frequencies. *J Neurosci*. 2012; 32:1395–1407. [PubMed: 22279224]
- Majeed W, Magnuson M, Hasenkamp W, Schwarb H, Schumacher EH, Barsalou L, Keilholz SD. Spatiotemporal dynamics of low frequency BOLD fluctuations in rats and humans. *Neuroimage*. 2011; 54:1140–1150. [PubMed: 20728554]
- Majeed W, Magnuson M, Keilholz SD. Spatiotemporal dynamics of low frequency fluctuations in BOLD fMRI of the rat. *J Magn Reson Imaging*. 2009; 30:384–393. [PubMed: 19629982]
- Mayer AR, Mannell MV, Ling J, Gasparovic C, Yeo RA. Functional connectivity in mild traumatic brain injury. *Hum Brain Mapp*. 2011; 32:1825–1835. [PubMed: 21259381]
- Mohajerani MH, Chan AW, Mohsenvand M, LeDue J, Liu R, McVea DA, Boyd JD, Wang YT, Reimers M, Murphy TH. Spontaneous cortical activity alternates between motifs defined by regional axonal projections. *Nat Neurosci*. 2013; 16:1426–1435. [PubMed: 23974708]
- Pan WJ, Thompson GJ, Magnuson ME, Jaeger D, Keilholz S. Infralow LFP correlates to resting-state fMRI BOLD signals. *Neuroimage*. 2013; 74:288–297. [PubMed: 23481462]
- Petridou N, Gaudes CC, Dryden IL, Francis ST, Gowland PA. Periods of rest in fMRI contain individual spontaneous events which are related to slowly fluctuating spontaneous activity. *Hum Brain Mapp*. 2013; 34:1319–1329. [PubMed: 22331588]
- Pizoli CE, Shah MN, Snyder AZ, Shimony JS, Limbrick DD, Raichle ME, Schlaggar BL, Smyth MD. Resting-state activity in development and maintenance of normal brain function. *Proc Natl Acad Sci U S A*. 2011; 108:11638–11643. [PubMed: 21709227]
- Raichle ME. The restless brain. *Brain Connect*. 2011; 1:3–12. [PubMed: 22432951]
- Raichle ME, Snyder AZ. A default mode of brain function: a brief history of an evolving idea. *Neuroimage*. 2007; 37:1083–1090. discussion 1097–1089. [PubMed: 17719799]
- Sakoglu U, Pearlson GD, Kiehl KA, Wang YM, Michael AM, Calhoun VD. A method for evaluating dynamic functional network connectivity and taskmodulation: application to schizophrenia. *MAGMA*. 2010; 23:351–366. [PubMed: 20162320]

- Shmuel A, Leopold DA. Neuronal correlates of spontaneous fluctuations in fMRI signals in monkey visual cortex: Implications for functional connectivity at rest. *Hum Brain Mapp.* 2008; 29:751–761. [PubMed: 18465799]
- Smyser CD, Snyder AZ, Neil JJ. Functional connectivity MRI in infants: exploration of the functional organization of the developing brain. *Neuroimage.* 2011; 56:1437–1452. [PubMed: 21376813]
- Stevens WD, Hasher L, Chiew KS, Grady CL. A neural mechanism underlying memory failure in older adults. *J Neurosci.* 2008; 28:12820–12824. [PubMed: 19036975]
- Swanson, LW. *Brain Maps: Structure of the Rat Brain.* Elsevier; 2004.
- Tagliazucchi E, Balenzuela P, Fraiman D, Chialvo DR. Criticality in largescale brain FMRI dynamics unveiled by a novel point process analysis. *Front Physiol.* 2012a; 3:15. [PubMed: 22347863]
- Tagliazucchi E, von Wegner F, Morzelewski A, Brodbeck V, Laufs H. Dynamic BOLD functional connectivity in humans and its electrophysiological correlates. *Front Hum Neurosci.* 2012b; 6:339. [PubMed: 23293596]
- Thompson GJ, Merritt MD, Pan WJ, Magnuson ME, Grooms JK, Jaeger D, Keilholz SD. Neural correlates of time-varying functional connectivity in the rat. *Neuroimage.* 2013; 83:826–836. [PubMed: 23876248]
- Thompson GJ, Pan WJ, Magnuson ME, Jaeger D, Keilholz SD. Quasiperiodic patterns (QPP): large-scale dynamics in resting state fMRI that correlate with local infraslow electrical activity. *Neuroimage.* 2014; 84:1018–1031. [PubMed: 24071524]
- Tian L, Jiang T, Wang Y, Zang Y, He Y, Liang M, Sui M, Cao Q, Hu S, Peng M, Zhuo Y. Altered resting-state functional connectivity patterns of anterior cingulate cortex in adolescents with attention deficit hyperactivity disorder. *Neurosci Lett.* 2006; 400:39–43. [PubMed: 16510242]
- van Meer MP, Otte WM, van der Marel K, Nijboer CH, Kavelaars A, van der Sprenkel JW, Viergever MA, Dijkhuizen RM. Extent of bilateral neuronal network reorganization and functional recovery in relation to stroke severity. *J Neurosci.* 2012; 32:4495–4507. [PubMed: 22457497]
- Vertes RP. Differential projections of the infralimbic and prelimbic cortex in the rat. *Synapse.* 2004; 51:32–58. [PubMed: 14579424]
- Wang J, Zuo X, He Y. Graph-based network analysis of resting-state functional MRI. *Front Syst Neurosci.* 2010; 4:16. [PubMed: 20589099]
- Whitfield-Gabrieli S, Thermenos HW, Milanovic S, Tsuang MT, Faraone SV, McCarley RW, Shenton ME, Green AI, Nieto-Castanon A, LaViolette P, Wojcik J, Gabrieli JD, Seidman LJ. Hyperactivity and hyperconnectivity of the default network in schizophrenia and in first-degree relatives of persons with schizophrenia. *Proc Natl Acad Sci U S A.* 2009; 106:1279–1284. [PubMed: 19164577]
- Wiggins JL, Bedoyan JK, Peltier SJ, Ashinoff S, Carrasco M, Weng SJ, Welsh RC, Martin DM, Monk CS. The impact of serotonin transporter (5-HTTLPR) genotype on the development of resting-state functional connectivity in children and adolescents: a preliminary report. *Neuroimage.* 2012; 59:2760–2770. [PubMed: 22032950]
- Zhang N, Rane P, Huang W, Liang Z, Kennedy D, Frazier JA, King J. Mapping resting-state brain networks in conscious animals. *J Neurosci Methods.* 2010; 189:186–196. [PubMed: 20382183]

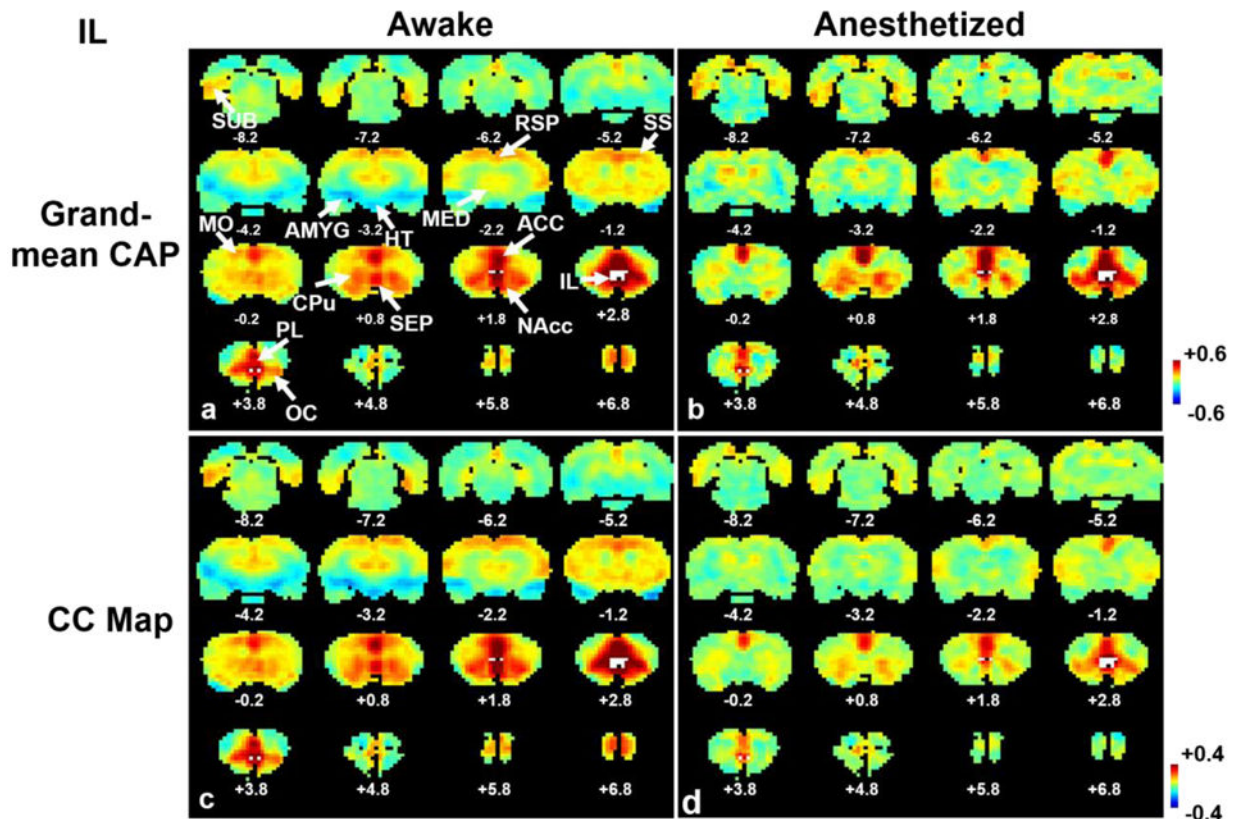


Figure 1.

Averages of 15% rsfMRI frames closely resembled RSFC maps obtained by correlational analysis for the seed of IL. a) Grand mean co-activation map in the awake state; b) grand mean co-activation map in the anesthetized state; c) seed correlation map in the awake state; d) seed correlation map in the anesthetized state. Distance to Bregma is marked at the bottom of each slice. The seed region of IL is labelled in white. Color bars in standard deviation (SD) in a and b, or in correlation coefficient in c and d. ACC, anterior cingulate cortex; RSP, retrosplenium; SUB, subiculum; SS, somatosensory, MO, motor; PL, prelimbic; OC, orbital cortices; CPu, caudate-putamen; HT, hypothalamus; AMYG, amygdala; MED, medial dorsal thalamus; NAcc, nucleus accumbens.

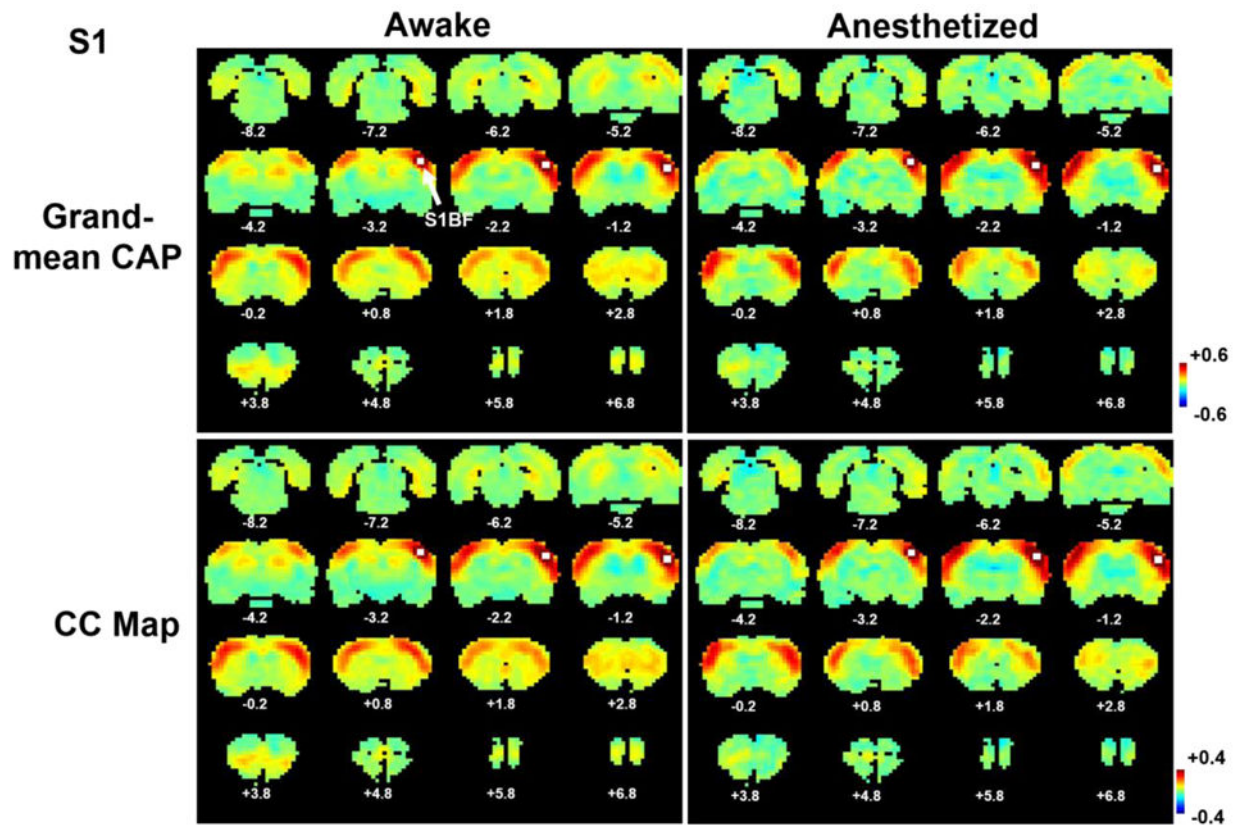


Figure 2.

Averages of 15% rsfMRI frames closely resembled RSFC maps obtained by correlational analysis for the seed of S1BF. a) Grand mean co-activation map in the awake state; b) grand mean co-activation map in the anesthetized state; c) seed correlation map in the awake state; d) seed correlation map in the anesthetized state. Distance to Bregma is marked at the bottom of each slice. The seed region of S1BF is labelled in white. Color bars in standard deviation (SD) in a and b, or in correlation coefficient in c and d.

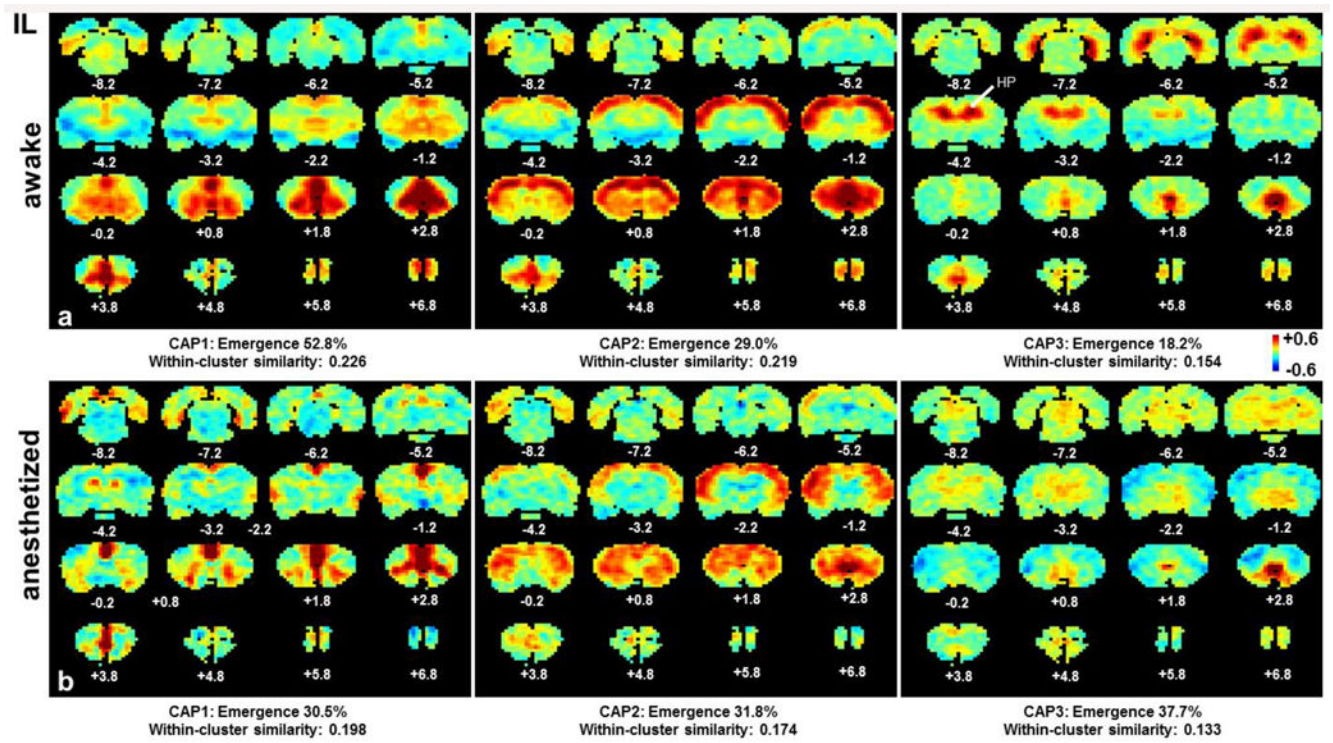


Figure 3. Individual CAPs of the IL network in awake and anesthetized states. a) CAPs 1-3 in the awake state; b) CAPs 1-3 in the anesthetized state. Distance to Bregma is marked at the bottom of each slice. Color bars in standard deviation (SD). Color bar applies for both states.

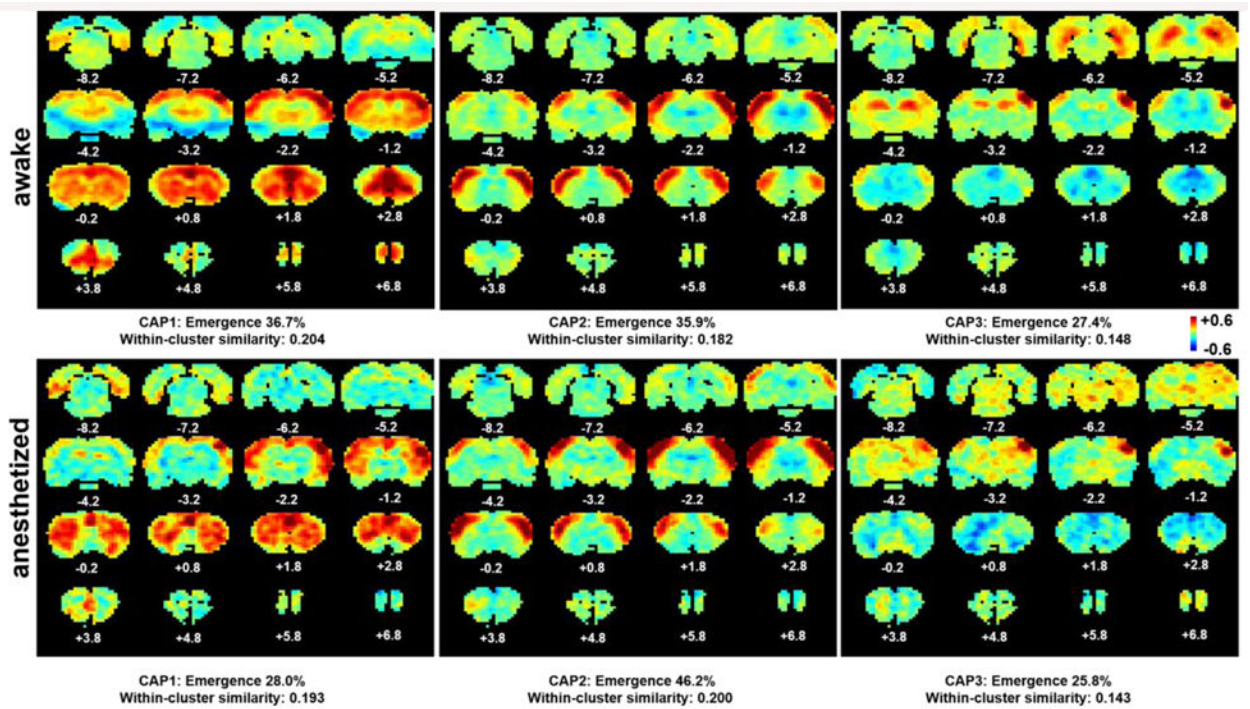


Figure 4. Individual CAPs of the S1BF network in awake and anesthetized states. a) CAPs 1-3 in the awake state; b) CAPs 1-3 in the anesthetized state. Distance to Bregma is marked at the bottom of each slice. Color bars in standard deviation (SD). Color bar applies for both states.

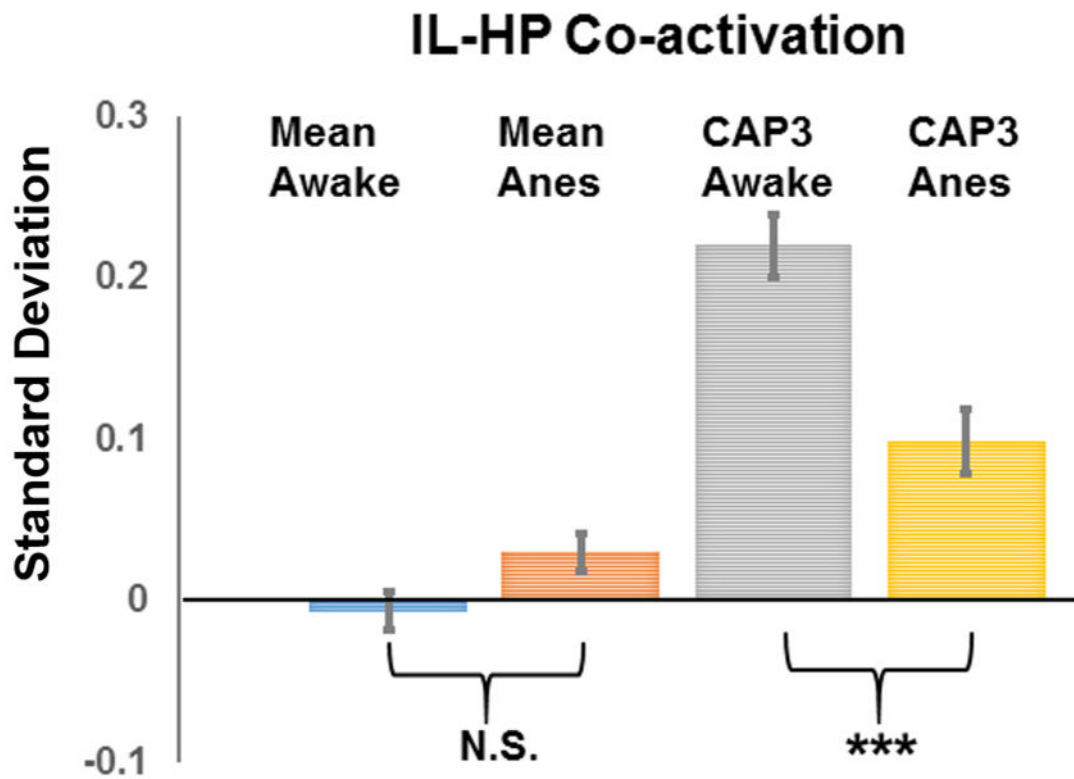


Figure 5. IL-HP co-activations in the grand-mean CAP and CAP3 in awake and anesthetized states. Significant co-activations were observed in CAP3 in both awake and anesthetized states but not in grand-mean CAPs. In addition, CAP3 was more sensitive for revealing anesthesia-induced IL-HP co-activation change than grand-mean CAPs. Error bars in standard error of mean (SEM). Y axis, mean signal intensity in standard deviation (SD).

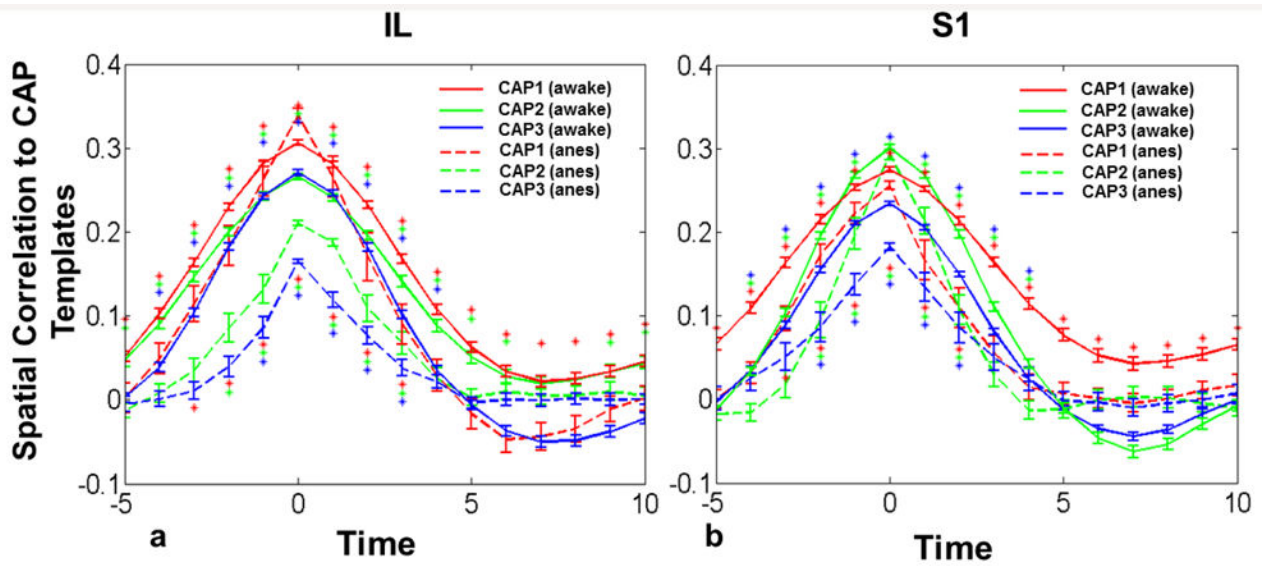


Figure 6.

Temporal evolutions of individual CAPs at both awake and anesthetized states. a) Temporal evolutions of IL CAPs; b) temporal evolutions of S1BF CAPs. X axis, time in seconds. Y axis, spatial correlation coefficients. Error bars in standard error of mean (SEM). Asterisks denote significant spatial correlation (one sample t test, $p < 0.01$, Bonferroni corrected). Asterisks above lines, statistical significance for the awake data. Asterisks below lines, statistical significance for the anesthetized data.

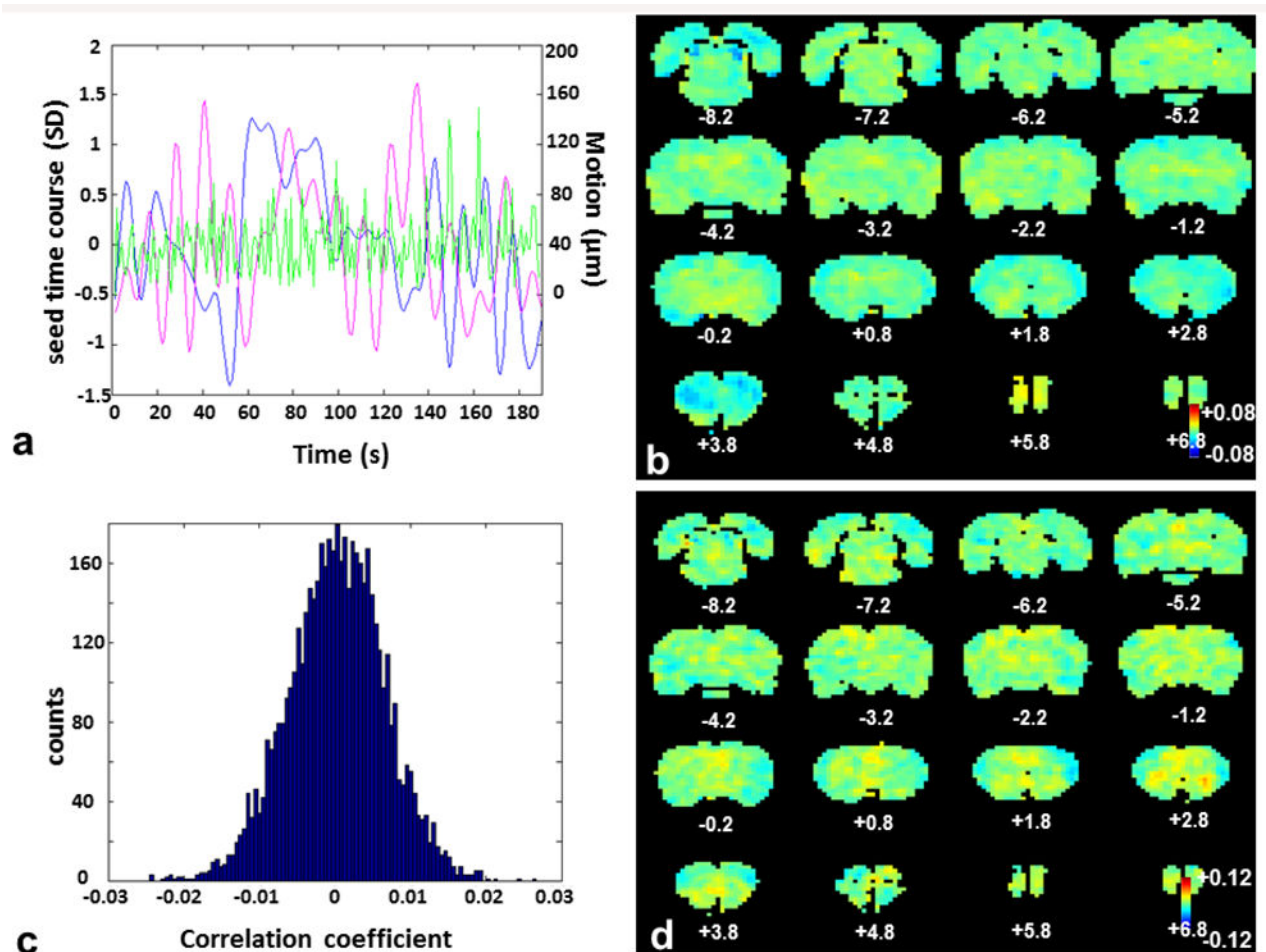


Figure 7.

Correlation between volume-to-volume movement and BOLD signals across the brain. a) A representative plot of the IL seed time course (blue), SIBF seed time course (magenta) and volume-to-volume displacement (green) from a randomly selected rsfMRI scan (i.e. single run). SD, standard deviation. b) Mean correlation map between unfiltered voxel time courses (i.e. with all preprocessing steps except for temporal filtering) and volume-to-volume displacement. c) Histogram of averaged correlation coefficients between voxel time courses and volume-to-volume displacement. d) Grand-mean CAP from 15% rsfMRI frames with the largest volume-to-volume displacement. Results of b, c and d are from the entire awake rat rsfMRI dataset. Note the color scales of b and d are five times smaller than the corresponding color scales in Figures 1 and 2.